Experimental observation of resonance manifold shrinking under zonal flow shear

T. Ullmann,[1,*] B. Schmid,[1] P. Manz,[2,3] B. van Milligen,[4] G.E.M. Tovar,[1] and M. Ramisch[1]

[1] *Institute for Interfacial Process Engineering and Plasma Technology IGVP, Universität Stuttgart, 70569 Stuttgart, Germany*
[2] *Max-Planck-Institut für Plasmaphysik, 85748 Garching, Germany*
[3] *Physik-Department E28, Technische Universität München, 85747 Garching, Germany*
[4] *EURATOM-CIEMAT, 28040 Madrid, Spain*

(Dated: September 14, 2020)

In two-dimensional turbulent systems the redistribution of energy can be described by quadratic non-linear three-wave interactions, which are limited by resonance conditions. The set of coupling modes can be understood as resonant manifold. It has been predicted by theory that in the presence of a shear flow the resonant manifold in wavenumber space shrinks in time favoring large scale structures. The phenomenon of manifold shrinking in the presence of shear flows is studied the first time experimentally in drift wave turbulence at the stellarator TJ-K by bicoherence analysis. By estimating effective mode numbers characterizing the width of the manifold, it is demonstrated that increasing shear leads to a shrinking of the resonance manifold.

In wave turbulence the nonlinear interaction can be approximately described by resonant N-wave interactions, where the resonance is restricted by the dispersion relation of the wave [1]. Sheared flows can impact the resonance of the wave coupling process. In turbulent 2D systems, as, e.g., MHD turbulence in the plane transverse to the external magnetic field [2, 3] and Rossby waves in the atmosphere [4, 5], mesoscopic shear flows are generated by a self-enhancing mechanism akin to an inverse cascade process. A prominent example is the zonal flow (ZF) which reacts back on the turbulence and suppresses its own driver, leading to predator-prey-like limit cycle oscillations [6, 7]. These large-scale flows can regulate turbulent transport perpendicular to their flow direction [8, 9]. For magnetized fusion plasmas it is believed that ZFs could play an important role in the formation of the transport barrier, which manifests itself in a strong stationary shear flow in the edge of the confined region, during the transition from low to high confinement regime [10–14]. Therefore, the effect of shear flows on the turbulence and their nonlinear wave interaction becomes the focus of attention. In this work, for the first time, the effect of self generated sheared flows (ZFs) on the resonant three-wave interaction of drift waves is studied experimentally. For this investigation, the temporal evolution of the resonance coupling manifold is resolved in wavenumber space enabled by measurements with a probe array in the low-temperature plasmas of stellarator experiment TJ-K [15]. We find that the resonance manifold shrinks with increasing shear and extends back when the shear vanishes. The experimental results agree well with model calculations relying on experimental shear data.

Drift-wave turbulence can be described by the Hasegawa-Wakatani equations [16] or, in the adiabatic limit, by the Hasegawa-Mima equation [17]. A Fourier transformation leads to the wave-coupling equation

$$\partial_t \hat{\phi}_{\mathbf{k}_3} + i\omega(\mathbf{k}_3)\hat{\phi}_{\mathbf{k}_3} = \frac{1}{2}\sum_{\mathbf{k}_1+\mathbf{k}_2=\mathbf{k}_3} \Lambda_{\mathbf{k}_1,\mathbf{k}_2}\hat{\phi}_{\mathbf{k}_1}\hat{\phi}_{\mathbf{k}_2} \ , \quad (1)$$

with the nonlinear coupling term on the right-hand side originating from the convective derivative. Here, $\hat{\phi}_{\mathbf{k}_i}$ is the dimensionless potential in Fourier space and $\omega(\mathbf{k}_3)$ the drift wave dispersion relation. The potential is related to the flow by the $E \times B$ drift $\mathbf{v} = -\nabla\phi \times \mathbf{B}/B^2$. The coupling coefficient $\Lambda_{\mathbf{k}_1,\mathbf{k}_2} = \mathbf{k}_1 \times \mathbf{k}_2 \cdot \mathbf{z}\left(k_2^2 - k_1^2\right)/(1+k_3^2)$ determines the strength and direction of the individual couplings. The constraint, under which coupling takes place, is

$$\mathbf{k}_1 + \mathbf{k}_2 = \mathbf{k}_3 \ , \quad (2)$$

the resonance condition for three-wave interaction. It expands to the resonance condition in frequency space, $\omega(\mathbf{k}_1) + \omega(\mathbf{k}_2) - \omega(\mathbf{k}_3) = \Delta\omega \approx 0$, via the dispersion relation $\omega(\mathbf{k}_i) = k_{i,y}/(1+k_i^2)$, and limits the set of possible couplings in k-space [18]. Thus, for a specific mode only a distinct coupling space is permitted, the resonant manifold. The theoretical effect of flow shear on the manifold is examined by Gürcan [19]. The implementation of a constant shear v' in x-direction, i.e. flow in y-direction, leads to a time dependent k_x-component,

$$k'_{i,x} = k_{i,x} - v'\tau k_{i,y} \quad \text{with} \quad \tau = t + t_0 \ . \quad (3)$$

The initial time t_0 can be chosen freely. Equation (3) enters the dispersion relation such that the coupling space is reduced with increasing time. Therefore, small scale turbulent structures are forced to couple to the large flow structures, especially the ZF [19]. It is argued that this is the mechanism behind large-scale structure formation in quasi 2D turbulent systems [20], such as atmospheric turbulence or plasma turbulence in toroidal fusion devices. ZFs ($k_y = 0$) hold a special position as they satisfy the resonance condition (2) in a trivial way. These

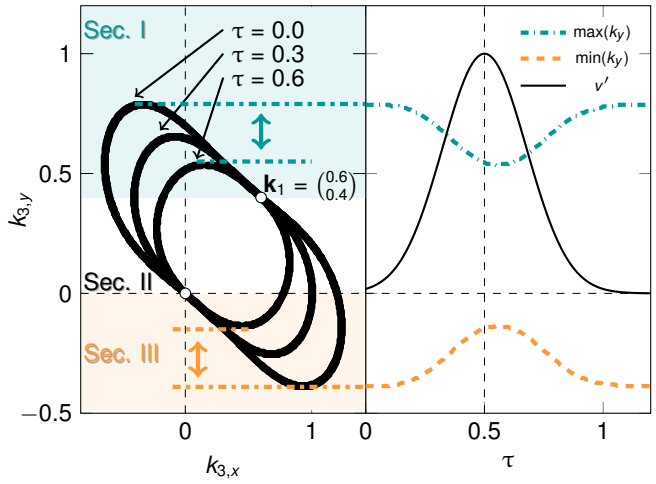

FIG. 1. Illustration of the effect of shear flow on the extent of the resonance manifold. *Left:* The manifold (black band), $\mathbf{k}_1 = (0.6, 0.4)$ coupling with $\mathbf{k}_3$, shrinks with time τ in sections I and III. *Right:* A temporal varying shear v' (black solid line) leads to a dip in the extent of the manifold with respect to $k_{3,y}$.

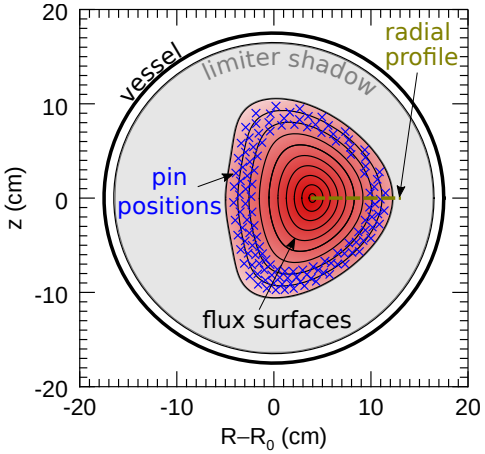

FIG. 2. Schematic cross section of TJ-K visualizing the experimental setup. For better comparison measurement positions are shown in the same plane. The probe array (blue cross) is positioned in the edge of the confined region. With a movable probe system radial profiles are obtained from the plasma center across the separatrix.

mesoscopic turbulent flows are, therefore, always part of the resonance manifold as persisting component coupling with the drift waves. As being shear flows themselves, this leads to a self-amplification of the ZF and a suppression of the primary instability. Physically, the mechanism is similar to the straining-out process of eddies, which explains the turbulence suppression by tilting and incorporation, rather than a breakup, of the vortices [14, 21]. Also when the background shear is controlled externally, e.g. by plasma biasing, ZF drive is enhanced as the time averaged resonant manifold is effectively weakened.

In order to account for dynamic variations in the flow shear, for comparison with the experiment, the coupling manifold is recalculated for a flow shear modelled as $v'(\tau) \propto \exp(-\tau^2)$. The effect on the resonance manifold is illustrated in Fig. 1. For the specific mode $\mathbf{k}_1 = (0.6, 0.4)$ the manifold is shown on the left side as a black band for the three time points $\tau = 0, 0.3$, and 0.6. With increasing time the manifold shrinks in its extent (marked as sec. I and III). Because of the stationary solutions of the ZF ($k_{2,y} = 0$, $k_{3,y} = 0$), the manifold does not shrink further into sec. II. From Fig. 1 (right), it can be seen that for finite lifetimes of the shear also the shrinking effect is temporally limited, which allows for analyses of manifold shrinking in correlation with zonal potential events. Since flow shear takes effect over time, a time lag between maximum shear as precursor and maximum shrinking may be expected from Fig. 1, too.

For a direct experimental test of the manifold shrinking effect the turbulent fluctuations have to be resolved in k-space. At the stellarator experiment TJ-K fluctuations in the floating potential can be accessed in wavenumber and frequency space, simultaneously, by means of multi-probe configurations. The low-temperature plasmas allow the use of Langmuir probes throughout the plasma, making it possible to acquire long time traces (2^{20} samples) with up to 1 MHz sampling frequency. As temperature fluctuations are small in TJ-K [22], fluctuations in the floating potential can be associated with plasma potential fluctuations, i.e. $\tilde{\phi}_{\mathrm{fl}} \approx \tilde{\phi}_{\mathrm{pl}}$. For the current analysis, a poloidal probe array was used consisting of 128 Langmuir probes positioned in the edge of the confined region. The probe positions are visualized in Fig. 2 as crosses. With a spatial uncertainty of 2 mm, the averaged poloidal probe spacing of $\Delta y \approx 1.55$ cm is well below the typical structure size of 3 to 5 cm [23–25]. For normalization the wavenumbers are multiplied by the drift scale, $\rho_{\mathrm{s}} = \sqrt{m_{\mathrm{i}} T_{\mathrm{e}}}/eB$, where the electron temperature T_{e} is obtained by a radially movable swept Langmuir probe (see Fig. 2). At a 2.45 Hz microwave frequency, corresponding to a magnetic field of $B = 72$ mT on axis, the hydrogen plasma is heated with 2.4 kW. This results in a maximum electron temperature of around $T_{\mathrm{e}} \approx 7$ eV and a line-averaged density of $\bar{n}_{\mathrm{e}} = 1.67 \cdot 10^{17} \mathrm{m}^{-3}$, with the latter determined from a microwave interferometer. It has been shown that the normalized quantities of TJ-K plasmas are similar to those in fusion edge plasmas [26] and turbulence is drift wave dominated [27, 28]. Two strong identifiers of drift-wave turbulence, which amongst others could be experimentally verified for TJ-K plasmas: A finite structure size $l_{\parallel}$ parallel to magnetic field lines with $l_{\parallel} \gg l_{\perp}$ [28] and $l_{\perp}$ typical perpendicular length scales of turbulent structures as well as a zero phase delay between density and potential fluctuations in a broad range of spatial scales [27]. The cross-phase results from the adiabatic parallel response of electrons to

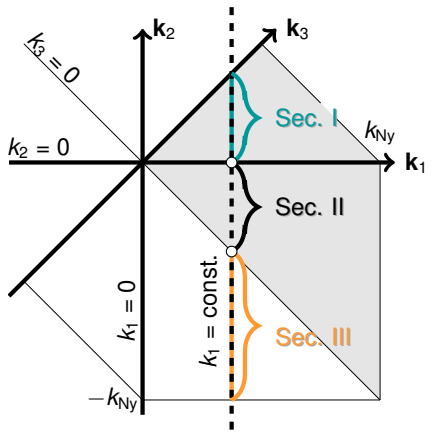

FIG. 3. Scheme of the bicoherence spectrum in k-space, where the projection of the resonance manifold on k_y can be identified (see text for further information). For a specific wavenumber k_1 = const. the manifold (dashed line) is suspected to shrink in section I (positive wavenumbers) and section III (negative wavenumbers).

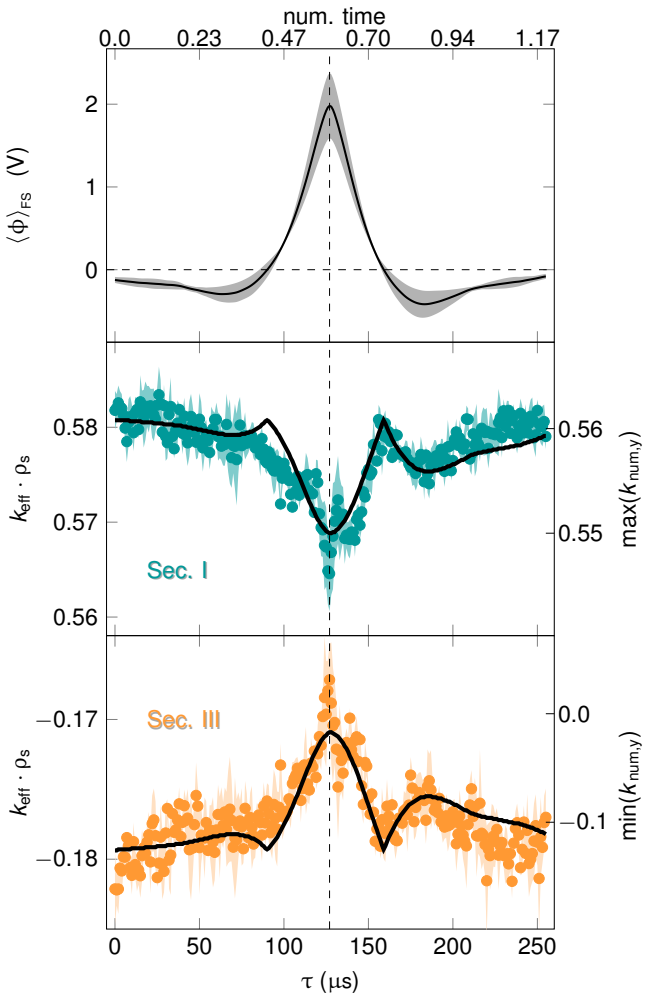

FIG. 4. Measurement of the effective extent of the resonant manifold during ZF occurrence. *Top:* Conditionally averaged ZF potential with uncertainty (light grey), which evolution can be regarded equivalent to the radial shear. *Below:* Time evolution of the effective wavenumber k_{eff} in section I (*middle*) and section III (*bottom*) shown as filled dots and uncertainty. Both time traces exhibit a drop of the effective wavenumber when the shear increases. The results are compared to numerical calculations (black solid lines).

the density perturbation. Self-generated flows have been detected as zonally averaged time varying potential perturbations [29]. Scans in the poloidal cross section and probe array measurements reveal their spatial structure and turbulent Reynolds stress drive [30]. In particular their radial localization gives rise to sheared zonal flows. This makes the experiment ideal for comparison with the theory presented above.

An experimental proof of the change in coupling manifold turns out to be quite challenging since the dispersion relation is subject to statistical scatter. Therefore, the coupling space itself is analyzed by a bicoherence spectrum in wavenumber and frequency space. This method intrinsically represents three-wave interactions which follow the resonance condition (Eq. (2)) in accordance with the dispersion relation. Due to the low spatial resolution in radial direction, only the size of the manifold in k_y is regarded and we refer to $k_{i,y}$ as k_i, from here on. The (auto) bicoherence applied on the potential fluctuations is

$$b^2(k_1,k_2,\omega_1,\omega_2,\tau) = \frac{|\langle\hat{\phi}_j(k_1,\omega_1,\tau)\hat{\phi}_j(k_2,\omega_2,\tau)\hat{\phi}_j^*(k_3,\omega_3,\tau)\rangle|^2}{\langle|\hat{\phi}_j(k_1,\omega_1,\tau)\hat{\phi}_j(k_2,\omega_2,\tau)|^2\rangle\langle|\hat{\phi}_j(k_3,\omega_3,\tau)|^2\rangle} \quad . \quad (4)$$

As the study of the coupling space requires a time dependent bicoherence, the coefficients $\hat{\phi}_j$ are calculated with a wavelet transformation [31], analogous to references [32]. The asterisk denotes the complex conjugate and $\langle\cdot\rangle$ the ensemble average. The triple product of the wavelet coefficients (numerator in Eq. (4)) is a measure of the phase coupling between the three components (k_1,ω_1), (k_2,ω_2), and (k_3,ω_3). For statistically independent modes, the sum of the individual phases average out and the bicoherence vanishes. With the normalization to the cross and auto power spectrum (denominator in Eq. (4)), the bicoherence is limited to the range $[0,1]$, resulting from the Cauchy-Schwarz inequality. The resultant bicoherence spectrum spans in a four-dimensional coupling space $(k_1,k_2,\omega_1,\omega_2)$. As we are interested in the extent of the manifold in k-space, the spectrum is averaged over all frequencies where the bicoherence is above the significance level, i.e. greater than $1/\sqrt{N}$ [33, 34], leading to the reduced bicoherence spectrum $b^2(k_1,k_2,\tau)$.In Fig. 3 a common representation of such a spectrum for a single time point is shown schematically. For discrete time traces the domain of definition is restricted to the out-

lined part. The wavenumbers k_1, k_2, and $k_3 = k_1 + k_2$ are limited to wavenumbers below the Nyquist wavenumber $\pm k_{\mathrm{Ny}}$. The diagonal and counter diagonal are distinguished with the requirement $k_1 - k_2 = 0$ and $k_1 + k_2 = 0$, respectively. Because of symmetry to these axes, i.e. $b^2(k_1, k_2) = b^2(k_2, k_1) = b^2(-k_1, -k_2)$ [35], only one quarter of the plane contains independent information (shaded area in Fig. 3). For an arbitrarily chosen mode k_1 all corresponding interactions are located on the vertical line $k_1 = \text{const.}$ (dashed line). This is the coupling manifold for the respective mode k_1 in a projection onto the k_y-axis (cf. Fig. 1). The points $k_2 = 0$ and $k_3 = 0$ (white dots) mark the interaction with the ZF. Hence, the sections described before can be identified in the bicoherence spectrum. The segment $k_2 > 0$ refers to section I, $0 \geq k_2 \geq -k_1$ to section II, and $k_2 < -k_1$ to section III. Only section I (positive wavenumbers) and III (negative wavenumbers) are of interest for the analysis of the shrinking effect, because only here a statement about the behavior of the manifold can be made. For each section an effective wavenumber k_{eff} is calculated as a measure for the width of the coupling space,

$$k_{\mathrm{eff}} = \sum_{\mathrm{k_2}} w(k_2) \cdot k_2 \quad \text{with} \quad w = \frac{b(k_2)}{\sum_{\mathrm{k_2}} b(k_2)} \quad . \qquad (5)$$

The weighting factor w accounts for the individual coupling strength each mode exhibits. High and low absolute values of k_{eff} indicate a broad and narrow coupling space, respectively.

To study the temporal evolution of the flow shear a conditional averaging technique is used to create the ensemble average in the calculation of the bicoherence (Eq. (5)). The ZF, regarded as poloidal shear flow, is linked to a coherent potential fluctuation on the complete flux surface ($k_\theta = 0$), which the experiment directly gives access to. Hence the zonal potential is used as trigger signal with the condition $+2\sigma$, triggering on the signal maximum as previously done in studies on related particle [29] and momentum [30] transport. With subwindows of 256 μs, the ensemble average is build from more than 1000 realizations to reflect the averaged dynamics around the ZF event. The temporal evolution of the zonal potential $\langle\phi\rangle_{\mathrm{FS}}$ is shown on the top of Fig. 4. For the quantification of the size of the coupling manifold, the effective wavenumber is calculated for each time point τ, according to Eq. (5). The evolution of $k_{\mathrm{eff}}(\tau)$ for $k_1\rho_s = 0.48$, as an example, is shown in Fig. 4 in the two lower plots for both of the meaningful sections. When the ZF advances, and thus the shear increases, the effective wavenumber in section I decreases. Vice versa, the effective wavenumber in section III increases, thus the manifold shrinks. The minimum extent is reached when the zonal potential is maximal ($\tau \approx 128\,\mu$s). A possible shift between both is small and hard to identify. This is due to the fact that the overall time duration of the ZF is short and the connected shear is relatively weak, with the same fluctuation amplitude as the ambient turbulence. At falling ZF amplitude the manifold increases again to the original size. The solid lines in the plots represent the shrinking that would be expected from the manifold shrinking model (Eq. (3)), using the time dependent experimental shear as estimated from the zonal potential in Fig. 4 (top). The initial wavenumber for the calculation is estimated to $\mathbf{k}\rho_s \approx (0.40, 0.48)$. Both time traces taken together reveal the drop in the size of the manifold, following the dynamics of the ZF. The temporal behaviour of the experimentally found effective wavenumbers agree qualitatively well with the model calculations.

In Summary, a reduction of the coupling manifold by shear flows has been experimentally observed for the first time. In wave turbulence, wave coupling takes place among modes of a resonant manifold in consequence of the waves' dispersion relation. According to Gürcan [19], this manifold in drift-wave turbulence is predicted to shrink under flow shear. A combined conditional wavelet-based bispectral analysis method in wavenumber and frequency space, applied to multiprobe measurements of the plasma potential in the stellarator experiment TJ-K, has been used to demonstrate that the resonant manifold indeed shrinks in correlation with occurring ZF activity. Physically, this corresponds to the straining-out process of eddies, in which the dynamics evolves in favour of large-scale structures. As a persisting contribution within the shrinking manifold, ZFs gain relative importance in the turbulence's three-wave interactions, which may be reflected in an enhanced efficiency in turbulence-flow energy transfer. Moreover, the mechanism is not limited to time varying flow shear but also applies to background shear flows as well, which demonstrates the important role equilibrium shear flows may play in the coupling process between small-scale turbulence and large-scale structures – in particular in the turbulence suppression and transport barrier formation scenario in magnetically confined fusion plasmas. In future steps, quantitative aspects of turbulence reduction as reflected in turbulent amplitudes or growth rates should be addressed in comparison with changes in the non-linear coupling behaviour.

* til.ullmann@igvp.uni-stuttgart.de

[1] S. Nazarenko, *Wave Turbulence*, Lecture Notes in Physics, Vol. 825 (Springer Berlin Heidelberg, Berlin, Heidelberg, 2011).
[2] C. S. Ng and A. Bhattacharjee, Physics of Plasmas **4**, 605 (1997).
[3] S. Galtier, S. V. Nazarenko, A. C. Newell, and A. Pouquet, Journal of Plasma Physics **63**, 447 (2000).
[4] D. Y. Manin and S. V. Nazarenko, Physics of Fluids **6**, 1158 (1994).

[5] A. Hasegawa, C. G. Maclennan, and Y. Kodama, Physics of Fluids **22**, 2122 (1979).
[6] P. H. Diamond, S.-I. Itoh, K. Itoh, and T. S. Hahm, Plasma Physics and Controlled Fusion **47**, R35 (2005).
[7] P. Manz, M. Ramisch, and U. Stroth, Physical Review E **82**, 056403 (2010).
[8] P. W. Terry, Reviews of Modern Physics **72**, 109 (2000).
[9] M. Leconte and R. Singh, Plasma Physics and Controlled Fusion **61**, 095004 (2019).
[10] G. D. Conway, C. Angioni, F. Ryter, P. Sauter, and J. Vicente, Physical Review Letters **106**, 065001 (2011).
[11] T. Estrada, T. Happel, L. Eliseev, López-Bruna, *et al.*, Plasma Physics and Controlled Fusion **51**, 124015 (2009).
[12] P. Manz, G. S. Xu, B. N. Wan, H. Q. Wang, *et al.*, Physics of Plasmas **19**, 072311 (2012).
[13] F. Wagner, The European Physical Journal H **43**, 523 (2018).
[14] M. Xu, G. R. Tynan, P. H. Diamond, C. Holland, *et al.*, Physical Review Letters **107**, 055003 (2011).
[15] N. Krause, C. Lechte, J. Stöber, U. Stroth, *et al.*, Review of Scientific Instruments **73**, 3474 (2002).
[16] A. Hasegawa and M. Wakatani, Physical Review Letters **50**, 682 (1983).
[17] A. Hasegawa and K. Mima, Physics of Fluids **21**, 87 (1978).
[18] W. Horton and A. Hasegawa, Chaos: An Interdisciplinary Journal of Nonlinear Science **4**, 227 (1994).
[19] Ö. D. Gürcan, Physical Review Letters **109**, 155006 (2012).
[20] A. M. Balk, V. E. Zakharov, and S. V. Nazarenko, Journal of Experimental and Theoretical Physics **71**, 446 (1990).
[21] P. Manz, M. Ramisch, and U. Stroth, Physical Review Letters **103**, 165004 (2009).
[22] N. Mahdizadeh, F. Greiner, M. Ramisch, U. Stroth, *et al.*, Plasma Physics and Controlled Fusion **47**, 569 (2005).
[23] M. Ramisch, N. Mahdizadeh, U. Stroth, F. Greiner, *et al.*, Physics of Plasmas **12**, 032504 (2005).
[24] G. Fuchert, G. Birkenmeier, B. Nold, M. Ramisch, *et al.*, Plasma Physics and Controlled Fusion **55**, 125002 (2013).
[25] G. Birkenmeier, M. Ramisch, G. Fuchert, A. Köhn, *et al.*, Plasma Physics and Controlled Fusion **55**, 015003 (2013).
[26] U. Stroth, F. Greiner, C. Lechte, N. Mahdizadeh, *et al.*, Physics of Plasmas **11**, 2558 (2004).
[27] C. Lechte, S. Niedner, and U. Stroth, New Journal of Physics **4**, 34 (2002).
[28] N. Mahdizadeh, F. Greiner, T. Happel, A. Kendl, *et al.*, Plasma Physics and Controlled Fusion **49**, 1005 (2007).
[29] G. Birkenmeier, M. Ramisch, B. Schmid, and U. Stroth, Physical Review Letters **110**, 145004 (2013).
[30] B. Schmid, P. Manz, M. Ramisch, and U. Stroth, New Journal of Physics **19**, 055003 (2017).
[31] C. Torrence and G. P. Compo, Bulletin of the American Meteorological Society **79**, 61 (1998).
[32] B. P. van Milligen, E. Sánchez, T. Estrada, C. Hidalgo, *et al.*, Physics of Plasmas **2**, 3017 (1995).
[33] R. A. Haubrich, Journal of Geophysical Research **70**, 1415 (1965).
[34] Z. Ge, Physical Review E **81**, 56311 (2010).
[35] Y. C. Kim and E. J. Powers, IEEE Transactions on Plasma Science **7**, 120 (1979).